Competition between S_N2 and Single Electron Transfer Reactions as a Function of Steric Hindrance Illustrated by the Model System AlkylCl + NO^-

Cyrille Costentin and Jean-Michel Savéant*

Contribution from the Laboratoire d'Electrochimie Moléculaire, Unité Mixte de Recherche Université, CNRS No 7591, Université de Paris 7-Denis Diderot, Case Courrier 7107, 2 place Jussieu, 75251 Paris Cedex 05, France

Received September 24, 1999

Abstract: The S_N2 reaction is a good example of the dichotomy and connection between electron-pair transfer chemistry and single electron transfer (ET) chemistry. Based on experimental stereochemical and kinetic data and on theoretical considerations, the dichotomy may be envisioned in two ways. One is competition between two distinct pathways, implying the existence of two distinct transition states on the potential energy hypersurface representing the reacting system, each connected to the S_N2 and ET products, respectively. The other considers a single transition state which could competitively give rise to both products. In both cases, steric hindrance is expected to favor the formation of the ET over the S_N2 products. An ab initio quantum chemical analysis of the model systems RCl + NO^-, with R = methyl, ethyl, isopropyl, and *tert*-butyl, taking account of electron correlation (at the MP2 level) and of solvation, shows the existence of distinct S_N2 and ET transition states. As steric hindrance increases, the S_N2 activation free energy increases while the ET activation free energy does not vary much. The result is that the balance favors more and more the ET reaction, which becomes predominant in the *tert*-butyl case. The geometries of the two transition states are drastically different, being characterized by a N, C, Cl atom sequence in the S_N2 transition state and a C, Cl, N sequence in the ET transition state. The looseness of its transition state and the lesser directionality of attack as compared to the S_N2 reaction are factors favorable to the ET reaction. An indirect ET pathway may follow the S_N2 transition state. Its importance increases with steric hindrance. The *tert*-butyl case represents an extreme situation where the S_N2 transition state is connected with the ET products rather than with the S_N2 products, while the direct ET pathway becomes more facile than the S_N2 pathway. All directions of attack lead to single electron transfer with similar activation energies, with similar reacting distances and negligible bonded interaction in the transition state. This reaction thus offers a good illustration of an outer-sphere process, as conceived in previous models of dissociative electron transfer.

The dichotomy and connection between electron-pair transfer chemistry and single electron transfer chemistry has been the object of many investigations and debates mostly centered around the S_N2 reaction. From an experimental standpoint, a starting observation was that alkyl halides may alkylate aromatic anion radicals prepared as ions pairs from the reaction of the parent aromatic compound with an alkali metal.[1] Successive stereochemical studies[2] concerned the reaction of the anion radical of anthracene electrochemically generated in *N,N′*-dimethylformamide (DMF) in the presence of a quaternary ammonium cation, with several optically active 2-octyl halides. Most of the product was found to be racemic. However, a small but distinct amount of inverted product was also detected (of the order of 10% and slightly dependent on the halogen atom). This observation was interpreted as indicating the existence of a competition between an S_N2 pathway, leading to the inverted product, and a single electron transfer pathway (ET), yielding the racemic product as depicted in Scheme 1.

Scheme 1

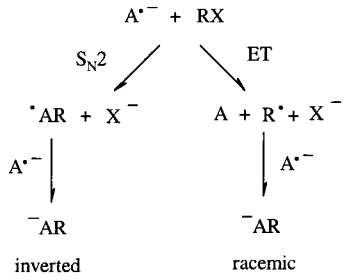

Further experimental studies involved the determination of the rate constant of the reaction of several alkyl halides with series of electrochemically generated anions radicals so as to construct activation driving force plots.[3] Such plots were used later to test the theory of dissociative electron transfer,[4] assuming, in view of the stereochemical data,[2] that the S_N2 pathway may be neglected in front of the ET pathway in their competition for controlling the kinetics of the reaction.

(1) (a) Garst, J. F. *Acc. Chem. Res*. **1971**, *4*, 400. (b) Bank, S.; Juckett, D. A. *J. Am. Chem. Soc.* **1976**, *98*, 7742.

(2) Herbert, E.; Mazaleyrat, J.-P.; Welvart, Z.; Nadjo, L.; Savéant, J.-M. *Nouv. J. Chem.* **1985**, *9*, 75.

(3) (a) Andrieux, C. P.; Gallardo, I.; Savéant, J.-M. *J. Am. Chem. Soc.* **1986**, *108*, 638. (b) Lund, H.; Lund, T. *Acta Chem. Scand. Ser. B* **1986**, *40*, 470. (c) Lund, H.; Lund, T. *Acta Chem. Scand. Ser.* B **1987**, *41*, 93.

(4) (a) Based on a Morse curve description of bond breaking in the reactant system and on a purely repulsive Morse curve description of bond breaking in the product system.[4b] (b) Savéant, J.-M. *J. Am. Chem. Soc.* **1987**, *109*, 6788. (c) Andrieux, C. P.; Savéant, J.-M.; Tardy, C. *J. Am. Chem. Soc.* **1998**, *120*, 4167.

10.1021/ja993467m CCC: $19.00
Published on Web 02/26/2000

Aromatic anion radicals thus appeared as prototypes of outer-sphere electron donors in dissociative electron transfer reactions, as they were considered to be in simple outer-sphere reactions where no bond is broken in concert with electron transfer. Based on this outer-sphere character, activation/driving force plots obtained with a series of aromatic anion radicals were used to judge the S_N2 or ET character of the reaction of an unknown nucleophile (viz., an electron donor) with the same cleaving acceptor according to a kinetic advantage approach.[3c,5] In this connection, classical S_N2 reactions such as halide self-exchange reactions exhibit rate constants that are much larger than predicted from the ET activation/driving force plot, thus confirming unambiguously their S_N2 character.[6]

However, a more accurate comparison between the experimental reaction kinetics and the predictions of the dissociative electron transfer theory revealed that the agreement is good when steric hindrance is maximal (tertiary carbon acceptors) and that the reaction is increasingly faster than predicted as steric hindrance decreases.[7] These results were interpreted as indicating an increase of the ET character of the reaction as steric hindrance increases. Similar conclusions were drawn from the temperature dependence of the kinetics, which revealed that the entropy of activation increases with steric hindrance, paralleling the increase of the ET character of the reaction.[5b,8]

From these experimental data and/or from general considerations, two conceptions of the S_N2/ET dichotomy and of the passage between one mechanism and the other have emerged. One involves competition between two distinct pathways, implying the existence of two distinct transition states on the potential energy hypersurface representing the reacting system, each connected to the S_N2 and ET products, respectively.[2,5b,7,9] The S_N2 pathway is accordingly favored in terms of energy by bonded interactions in the transition state that do not exist in the ET transition state. However, the latter has a looser structure and the ET reaction is less demanding in terms of directionality (front, back, and side attacks involve activation energies of similar magnitude). The ET pathway thus possesses an entropy advantage over the S_N2 pathway. The effect of steric hindrance is to diminish the energy gain offered by bonded interactions in the S_N2 transition state and thus to favor the ET pathway.

The other view is that the ET and S_N2 mechanisms are the ends of a continuous mechanistic spectrum, implying that a single transition state is to be found on the potential energy hypersurface of the reacting system.[3b,10,11] As pointed out earlier,[7] entropy factors are, along with energy factors, essential to the description of the reactions dynamics and product distribution. An extremely detailed analysis of the problem has been carried out in the framework of a Morse curve model of the reaction,[12] generalizing a previous Morse curve model of dissociative electron transfer reactions.[4b]

Several ab initio quantum chemical studies have been carried out on simple systems, much simpler than the experimental systems, aiming at determining which of the two conceptions evoked earlier best represents the course of this type of reaction. Contrasting results were obtained, leading to diverging conclusions.[13] One example is the reaction of $H_2CO^{\bullet -}$ with CH_3Cl, which leads to electron transfer products ($H_2CO + CH_3^{\bullet} + Cl^-$) and to two types of substitution products deriving from O-substitution ($H_2COCH_3^{\bullet} + Cl^-$) and C-substitution ($^{\bullet}OCH_2$-$CH_3 + Cl^-$), respectively. One study finds an O- and a C-substitution transition state.[14a] The first transition state leads to the O-substitution product, while the second is connected to electron transfer products by a reaction path obtained with ROHF calculations in non-mass-weighted coordinates. In a second study of the same system,[14b] three transition states are found, namely the same O- and C-substitution transition states as before and, in addition, an outer-sphere electron transfer transition state. Following the steepest descent reaction pathways by the IRC method (see the Methodology section) with UHF calculations in mass-weighted coordinates revealed that all three transition states are connected to the corresponding products. The same behavior was found with two other model systems namely, $H_2CO^{\bullet -} + CH_3F$ and $H_2C{=}CH_2^{\bullet -} + CH_3F$.[14b]

Further investigations indicated that, after passing through the C-substitution transition state, the system may bifurcate[15] and partition between the C-substitution products and the ET products.[14c] The structure of the potential energy hypersurface in the vicinity of the C-substitution transition state and the very fact that the IRC−UHF pathway in mass-weighted coordinates leads to the C-substitution products, however, indicate that the percentage of ET products obtained by this mechanism should be much smaller than the percentage of C-substitution products.

In a recent study,[14d] the effect of steric hindrance is treated in the framework of a mechanism in which a bifurcation follows the passage through an S_N2-like transition state. Bifurcation then appears to be increasingly favorable to the ET products as steric hindrance increases. The S_N2 and ET reactions would thus have a common transition state (the S_N2 transition state), and product selection would be the result of a bifurcation following the transition state. The effect of steric hindrance would thus be to increase the energy of the common transition state and to make the bifurcation increasingly favorable to the ET reaction. These views contrast earlier results[14b] in the sense that they do not take into account the existence of an outer-sphere ET pathway going through a distinct ET transition state. Even if it is true

(5) (a) Lexa, D.; Mispelter, J.; Savéant, J.-M. *J. Am. Chem. Soc.* **1981**, *103*, 6806. (b) Lexa, D.; Savéant, J.-M.; Su, K. B.; Wang, D. L. *J. Am. Chem. Soc.* **1988**, *110*, 7617. (c) Lund, H.; Lund, T. *Acta Chem. Scand. Ser. B* **1988**, *42*, 269. (d) Tolbert, L. M.; Bedlek, J.; Terapane, M.; Kowalik, J. *J. Am. Chem. Soc.* **1997**, *119*, 2291.

(6) Eberson, L. *Electron Transfer in Organic Chemistry*; Springer-Verlag: Heidelberg, 1987.

(7) Savéant, J.-M. *J. Am. Chem. Soc.* **1992**, *114*, 10595.

(8) (a) Daasberg, K.; Petersen, S. U.; Lund, H. *Acta Chem. Scand.* **1991**, *45*, 470. (b) Andrieux, C. P.; Delgado, G.; Savéant, J.-M. *J. Electroanal. Chem.* **1993**, *448*, 141.

(9) Savéant, J.-M. Single Electron Transfer and Nucleophilic Substitution. In *Advances in Physical Organic Chemistry*; Bethel, D., Ed.; Academic Press: New York, 1990; Vol. 26, pp 1−130.

(10) (a) Lund, H.; Lund, T. *Acta Chem. Scand. Ser. B* **1988**, *42*, 269. (b) Pross, A. A General Approach to Organic Reactivity: The Configuration Mixing Model. In *Advances in Physical Organic Chemistry*; Bethel, D., Ed.; Academic Press: New York, 1985; Vol. 21, pp 99−196.

(11) (a) In line with this conception is the contention that, with very few exceptions, homogeneous electron transfer reactions should be regarded as inner-sphere rather than outer-sphere processes with strongly avoided crossing energies and tight geometries of their transition state.[11b,c] (b) Eberson, L.; Shaik, S. S. *J. Am. Chem. Soc.* **1990**, *112*, 4484. (c) Cho, J. K.; Shaik, S. S. *J. Am. Chem. Soc.* **1991**, *113*, 9890.

(12) Marcus, R. A. *J. Phys. Chem. A* **1997**, *101*, 4072.

(13) (a) For recent reviews, see refs 13b and c. (b) Speiser B. *Angew. Chem., Int. Ed. Engl.* **1996**, *35*, 2471. (c) Zipse, H. *Angew. Chem., Int. Ed. Engl.* **1997**, *36*, 1697.

(14) (a) Sastry, G. N.; Shaik, S. S. *J. Am. Chem. Soc.* **1995**, *117*, 3290. (b) Bertran, J.; Gallardo, I.; Moreno, M.; Savéant, J.-M. *J. Am. Chem. Soc.* **1996**, *118*, 5737. (c) Shaik, S. S., Danovich, D.; Sastry, G. N.; Ayala, P. Y.; Schlegel, H. B. *J. Am. Chem. Soc.* **1997**, *119*, 9237. (d) Sastry, G. N.; Shaik, S. S. *J. Am. Chem. Soc.* **1998**, *120*, 2131. (e) Yamakata, H.; Aida, M.; Dupuis, M. *Chem. Phys. Lett.* **1999**, *300*, 583.

(15) (a) For general analyses of mechanism bifurcation see refs 15b−g. (b) Garrett, B. C.; Truhlar, D. G.; Wagner, A. F.; Dunning, T. H. *J. Chem. Phys.* **1983**, *78*, 4400. (c) Valtazanos, P.; Ruedenberg, K. *Theor. Chim. Acta* **1986**, *69*, 281. (d) Baker, J.; Gill, P. M. W. *J. Comput. Chem.* **1988**, *9*, 465. (e) Bosch, E.; Moreno, M.; Lluch J. M.; Bertran, J. *Chem. Phys. Lett.* **1989**, *1604*, 543. (f) Natanson, G. A.; Garrett, B. C.; Truong, T. N.; Joseph, T.; Truhlar, D. G. *J. Chem. Phys.* **1991**, *94*, 7875. (g) Schlegel, H. B. *J. Chem. Soc., Faraday Trans.* **1994**, *90*, 1569.

that this ET transition state has a higher energy than the S_N2 transition state, the difference is less in terms of free energy, and one could guess that steric hindrance will favor increasingly the ET transition state, possibly making the corresponding pathway predominating with tertiary alkyl derivatives.

To examine whether the S_N2/ET dichotomy may be conceived in terms of competing pathways with distinct transition states and how steric hindrance governs the competition, we have investigated the reaction of NO^- with RCl, with R = methyl, ethyl, isopropyl, and *tert*-butyl.[16] We have, indeed, found that the localization of the ET transition state is easier with this electron donor than with the previously investigated anion radicals, thus allowing a full characterization of the S_N2 and ET dichotomy. This model reaction thus illustrates one of the central theoretical questions of chemical reactivity, namely the connection between single electron transfer and electron-pair transfer and how the passage between one and the other may take place.

Results and Discussion

We observed that electron correlation is important in the calculation of the activation parameters. In this respect, the MP2 level of calculation appeared to be a reasonable compromise between accuracy and computer time. Solvation also has an important effect. It would then be desirable to optimize the geometries and calculate the energies, including solvation energies, at the MP2 level. While this procedure remains tractable with methyl chloride, it becomes too time-consuming with the other members of the series. We thus adopt the following approach after validation in the CH_3Cl case. The geometries of the maxima and minima on the potential energy hypersurface are optimized in the gas phase at the UHF/6-31G* level. The free enthalpies in the gas phase, G_{UHF}, are obtained according to eq 1 after calculation of the frequencies at the same level (*E*, energies; elec for electronic; therm for thermal; *T*, temperature; *S*, entropy). The energies corresponding to these

$$G_{UHF} = E^{elec}_{UHF} + ZPE + E^{therm} - TS \qquad (1)$$

geometries are then calculated at the MP2/6-31G* level and the free enthalpies in the gas phase, G^{gp}, obtained from eq 2.

$$G^{gp} = G_{UHF} - E^{elec}_{UHF} + E^{elec}_{MP2} \qquad (2)$$

The free enthalpy of solvation, G^{solv}, was then calculated at the MP2 level by two dielectric continuum methods: the COSMO method and the IPCM method (see the Methodology section). All available solvation estimations are rather approximate, and we felt it was important to see whether the two methods give similar results. The free enthalpies, G^s, in solution are finally derived from eq 3. (In the calculation of the free

$$G^s = G^{gp} + G^{solv} + nRT\,[\ln(22.4) - 1] \qquad (3)$$

enthalpies, the reference state for the entropies corresponds to a volume of 1 L as opposed to the gas phase, where the reference state corresponds to a volume of 22.4 L). As observed for the example of the methyl derivative, the characteristic free enthalpies obtained at the MP2/6-31G*//UHF/6-31G* level are close to the more accurate values obtained at the MP2/6-31G* level, thus validating our simplified approach (see Appendix).

(16) (a) The reaction of NO^- with alkyl halides has been scarcely investigated experimentally. Reference 16b depicts the gas-phase reaction of NO^- with CH_3I and CCl_4. (b) Rinden, E.; Maricq, M. M.; Grabowski, J. J. *J. Am. Chem. Soc.* **1989**, *111*, 1203.

The most stable form of the electron donor, NO^-, is the triplet state, and so is the reactant system. The electron transfer product system, $R^\bullet + Cl^- + NO^\bullet$, is also a triplet state. This is not the case for the substitution product, R—N═O, whose most stable form is the singlet. For example, in the case of CH_3Cl, the singlet state of the substitution product is more than 1 eV more stable than the triplet state (see Appendix). However, as observed from a detailed analysis of the same CH_3Cl case, the triplet state is more stable than the singlet state for all points or portions of interest of the potential energy hypersurface where the competition between the two pathways takes place (see Appendix). This is the reason that all the calculations were performed for triplet states.

In all four cases, an S_N2 and an ET transition state were found without difficulty. Scheme 2 summarizes the geometries of the reactant and product systems and of the S_N2 and ET transition states (all structure details are given in the Supporting Information). The energetic and geometric characteristics of the various states of interest are summarized in Table 1 and the free enthalpy reaction profiles in Figure 1.

With regard to solvation energies, we see that the values found with COSMO are lower (in absolute value) than those found with IPCM but that the trends observed upon increasing steric hindrance are the same with both methods.[17]

The thermodynamics of the ET reaction, but also of the S_N2 reaction, do not vary much upon increasing steric hindrance. The systems under discussion therefore essentially provide an illustration of the effect of steric hindrance on transition states. It is also worth noting that, although the S_N2 product is more stable than the ET product in each case,[18] the difference in stability is not large (ca. 0.4 eV), thus providing a good opportunity for the ET pathway to compete successfully with the S_N2 pathway as steric hindrance increases. In this sense, albeit not an anion radical, NO^- behaves more like an anion radical than like a classical nucleophile leading to the formation of a strong bond.

In terms of free enthalpies, G^s (Figure 1), the S_N2 transition state is more stable than the ET transition state for the methyl derivative. As steric hindrance increases, the difference gets smaller. The free enthalpies of the two transition states are practically equal for the isopropyl derivative, while the balance turns in favor of the ET transition state for the *tert*-butyl derivative. The free enthalpies of activation are predicted to be very large, most probably too large. The dielectric continuum method used is, indeed, expected to overestimate the solvation energies, particularly for small ions such as NO^- and Cl^- involved in the presently investigated systems. As a consequence, the differences in solvation free enthalpies between the reactants and the transition states, which have quite different dimensions, are thus most probably overestimated. The actual activation free enthalpies in solution are thus most probably between the G^s and the $G^{gp} - 0.056$ values, albeit closer to the G^s values. The G^{gp} profiles[19] shown in Figure 1 display trends similar to those of the G^s profiles: as steric hindrance increases, the S_N2 pathway becomes increasingly less favorable, while the ET activation free enthalpy remains about the same.

(17) (a) A comparison between the two methods as applied to the S_N2 $CH_3Cl + Cl^-$ self-exchange reaction[17b] showed that the two methods reproduce correctly the experimental activation energies but that the COSMO method gives more reliable results when dealing with solvation along the whole reaction profile. (b) Truong, T. N.; Stefanovich, E. V. *J. Phys. Chem.* **1995**, *99*, 14700.

(18) As discussed later, the transition states are connected with reactant and product clusters that are more stable than the separated molecules. We nevertheless omit these clusters in the representation given in Figure 1 so as to make the total activation free enthalpies appear on the diagrams.

Scheme 2[a]

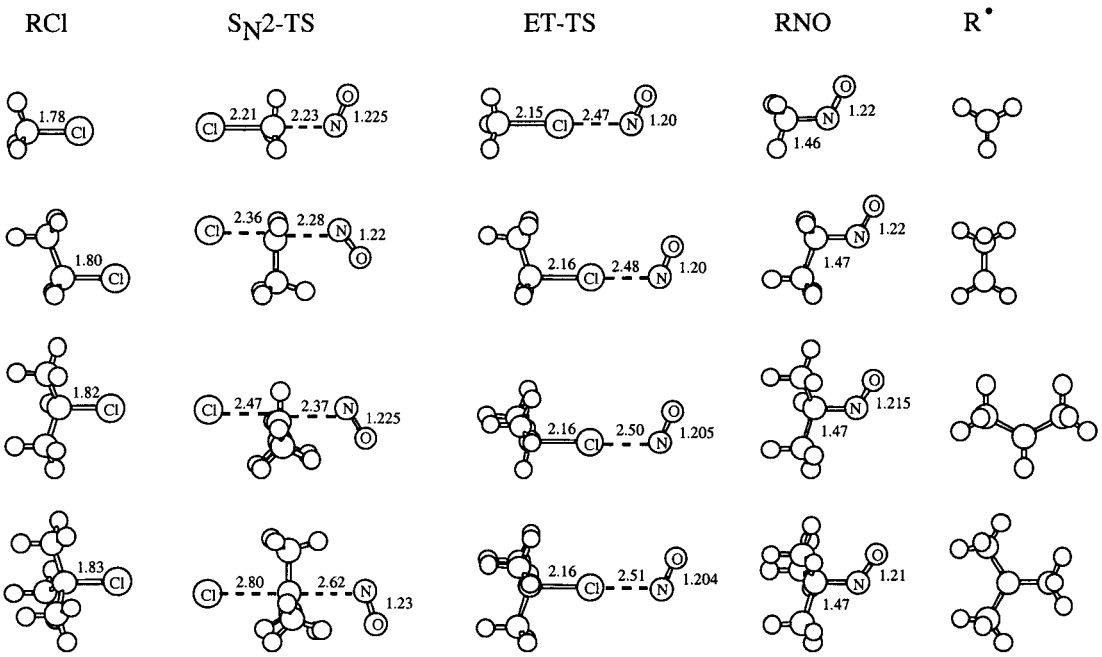

[a] S_N2-TS, S_N2 transition state; ET-TS, ET transition state. Distances in angstroms.

Table 1. Energetic and Geometric Characteristics of the Reactant, Product, and Transition-State Systems as a Function of Steric Hindrance[a]

	Me					Et				
	R	PS_N2	PET	S_N2-TS	ET-TS	R	PS_N2	PET	S_N2-TS	ET-TS
ΔE_{UHF}	0.00	−1.22	−0.70	−0.16	1.10	0.00	−1.22	−0.70	−0.13	1.03
ΔG_{UHF}	0.00	−1.09	−1.18	0.20	1.20	0.00	−1.09	−1.21	0.24	1.23
ΔE_{MP2}	0.00	−0.98	−0.20	−0.33	0.51	0.00	−0.96	−0.13	−0.27	0.54
ΔG^{gp}	0.00	−0.84	−0.62	−0.02	0.65	0.00	−0.83	−0.59	0.06	0.68
$G^{solv\ b}$	−2.85	−2.96	−2.71	−2.04	−2.50	−2.86	−2.93	−2.75	−2.06	−2.51
$G^{solv\ c}$	−3.37	−3.33	−3.18	−2.41	−2.70	−3.37	−3.33	−3.18	−2.34	−2.79
$\Delta G^{s\ a}$	0.00	−0.95	−0.48	0.79	1.00	0.00	−0.90	−0.48	0.86	1.03
$\Delta G^{s\ b}$	0.00	−0.80	−0.43	0.94	1.32	0.00	−0.79	−0.40	1.09	1.26
d_{C-Cl}	1.785	∞	∞	2.231	2.148	1.799	∞	∞	2.357	2.156
d_{C-N} or d_{Cl-N}	∞	1.457	∞	2.208	2.472	∞	1.466	∞	2.282	2.484
d_{N-O}	1.248	1.220	1.127	1.224	1.200	1.248	1.220	1.127	1.221	1.202
q_{N-O}	−1.00	−0.27	0.00	−0.80	−0.63	−1.00	−0.28	0.00	−0.78	−0.645
s_C	0.00	0.00	1.00	0.07	0.77	0.00	0.00	1.00	0.11	0.77
	i-Pr					*t*-Bu				
	R	PS_N2	PET	S_N2-TS	ET-TS	R	PS_N2	PET	S_N2-TS	ET-TS
ΔE_{UHF}	0.00	−1.325	−0.73	−0.11	1.015	0.00	−1.22	−0.79	0.02	0.965
ΔG_{UHF}	0.00	−1.08	−1.245	0.28	1.19	0.00	−1.08	−1.30	0.33	1.16
ΔE_{MP2}	0.00	−1.01	−0.09	−0.15	0.52	0.00	−1.06	−0.07	0.33	0.455
ΔG^{gp}	0.00	−0.77	−0.54	0.19	0.64	0.00	−0.91	−0.53	0.58	0.60
$G^{solv\ b}$	−2.85	−2.90	−2.735	−2.05	−2.51	−2.83	−2.86	−2.71	−2.20	−2.50
$G^{solv\ c}$	−3.38	−3.31	−3.18	−2.40	−2.86	−3.37	−3.30	−3.18	−2.50	−2.90
$\Delta G^{s\ a}$	0.00	−0.82	−0.42	0.99	0.98	0.00	−0.94	−0.41	1.21	0.93
$\Delta G^{s\ b}$	0.00	−0.71	−0.35	1.16	1.15	0.00	−0.84	−0.34	1.45	1.07
d_{C-Cl}	1.816	∞	∞	2.467	2.159	1.834	∞	∞	2.805	2.160
d_{C-N} or d_{Cl-N}	∞	1.475	∞	2.368	2.496	∞	1.485	∞	2.618	2.506
d_{N-O}	1.248	1.214	1.127	1.225	1.203	1.248	1.211	1.127	1.231	1.204
q_{N-O}	−1.00	−0.28	0.00	−0.80	−0.66	−1.00	−0.28	0.00	−0.84	−0.67
s_C	0.00	0.00	1.00	0.11	0.74	0.00	0.00	1.00	0.085	0.715

[a] The energies are in electronvolts and the distances in angstroms. ΔE_{UHF}, ΔG_{UHF}, ΔE_{MP2}, and ΔG are derived from the values of E_{UHF}, G_{UHF}, E_{MP2}, and G, calculated as explained in the text, by difference with the values corresponding to the reactant state. q_{N-O} is the charge borne by the NO moiety. s_C is the spin density on the reacting carbon. [b] The solvation free energy is calculated at the MP2 level, using the COSMO method. [c] The solvation free energy is calculated at the MP2 level, using the IPCM method.

Comparison between the two series of profiles shows that solvation reinforces the prevalence of the ET reaction over the S_N2 reaction, which appears upon increasing the steric hindrance.

The geometries of the S_N2 and ET transition states are strikingly different. While the nitrogen atom of the electron donor stands on the side of the central carbon opposite the chlorine atom in the former case, the chlorine stands between

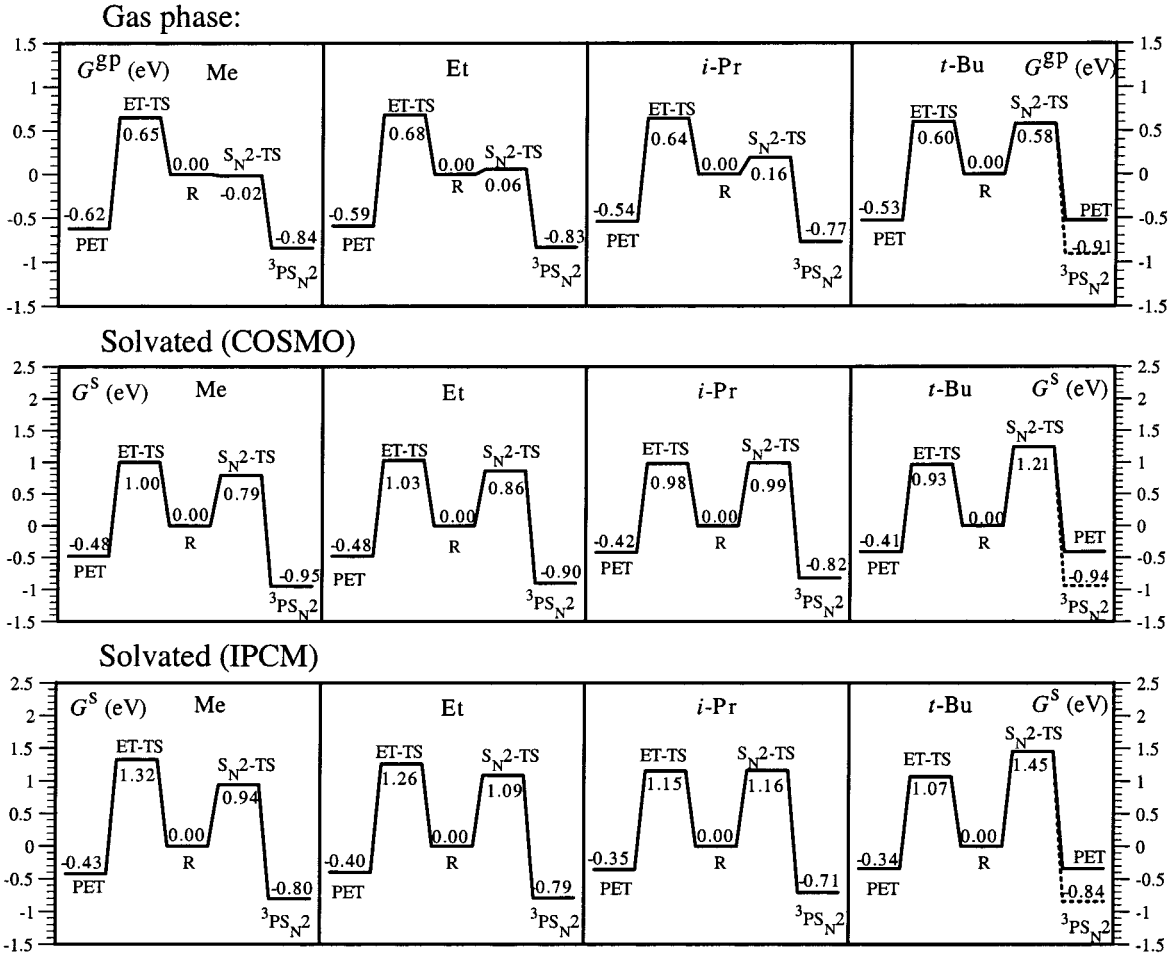

Figure 1. Energetic and geometric characteristics of the reactant, product, and transition state systems as a function of steric hindrance.

the reacting carbon and the nitrogen in the latter case. The S_N2-TS geometry reflects the interaction between the negative charge borne by the electron donor and the partial positive charge borne by the reacting carbon. In the ET-TS, the predominating factor is the overlap between the σ^* orbital of the C−Cl bond (mostly located on Cl) and the electrons on the NO^- nitrogen, which successfully fights electrostatic repulsion.

Related to this difference in structure is the fact that the geometry of the S_N2 transition state is quite sensitive to steric hindrance, whereas the chlorine−nitrogen and carbon−chlorine distances in the ET transition state are about the same over the whole series.

Another remarkable difference between the two transition states is the looser structure of the ET-TS as compared to the S_N2-TS in the sense that the characteristic normal-mode frequencies are smaller in the first case than in the second case. These differences in frequencies translate into differences in entropies in the following manner. The various molar entropic terms listed in Table 2 were calculated as follows:

$$S = S_{elec} + S_{trans} + S_{rot} + S_{vib} - R \ln N_A + R$$

(R, gas constant; N_A, Avogadro's number), with

(19) It may seem strange, at first, that the S_N2 transition states are endowed with negative energies. This is the result of the existence of a reactant cluster of lower energy than the separated reactants (R). The S_N2 transition state is thus higher in energy than the corresponding reactant cluster in all cases. Solvation makes all reactant clusters higher in energy than the separated reactants. This the reason that we did not show their geometric and energetic characteristics in Figure 1.

Table 2. Differences in Entropy[a] between the S_N2 and ET Transition States and the Reactant State.

		ΔS_{elec}	ΔS_{trans}	ΔS_{rot}	ΔS_{vib}	ΔS
Me	S_N2-TS	0.00	−1.24	−0.28	0.55	−0.97
	ET-TS	0.00	−1.24	−0.28	0.82	−0.70
Et	S_N2-TS	0.00	−1.25	−0.35	0.61	−0.99
	ET-TS	0.00	−1.25	−0.35	0.90	−0.69
i-Pr	S_N2-TS	0.00	−1.26	−0.38	0.61	−1.03
	ET-TS	0.00	−1.26	−0.38	1.04	−0.60
t-Bu	S_N2-TS	0.00	−1.26	−0.40	0.87	−0.78
	ET-TS	0.00	−1.26	−0.40	1.01	−0.65

[a] In millielectronvolts per mole per Kelvin. The reference state for the entropies corresponds to a volume of 1 L as opposed to the gas phase, where the reference state corresponds to a volume of 22.4 L.

$$S_{elec} = R \ln \omega_e$$

(ω_e is the multiplicity of the electronic state, $\omega_e = 3$ for a triplet)

$$S_{trans} = R\left\{\ln\left[\left(\frac{2\pi mkT}{h^2}\right)^{3/2} V\right] + \frac{3}{2}\right\}$$

(m is the mass of the system; V, the volume, is taken equal to 1 L)

$$S_{rot} = R\left\{\ln\left[\frac{\pi^{1/2}}{\sigma}\left(\frac{T}{\theta_A}\frac{T}{\theta_B}\frac{T}{\theta_C}\right)^{1/2}\right] + \frac{3}{2}\right\}$$

(σ is the symmetry number; T is the absolute temperature; the θ values are the rotational temperatures, related to the three inertia momenta along the three rotational axes)

$$S_{vib} = R\sum_{j=1}^{3n-6}\left[\frac{\theta_j/T}{e^{\theta_j/T}-1} - \ln(1-e^{\theta_j/T})\right]$$

where the vibrational temperatures, θ_j, are related to the corresponding frequencies, ν_j, according to $\theta_j = h\nu_j/k$ (h, Planck's constant; k, Boltzmann's constant).

The electronic contribution is nil because the reactant state and the two transition states are triplets. The translation contribution is negative because two particles are converted into one particle. It is the same for both transition states because their masses are the same. It becomes more negative from methyl to *tert*-butyl because the mass increases. The rotational contributions are close for the two transition states albeit not exactly the same (as observed when more figures are retained). This is because the overall shape and dimensions of the two transition states are similar. They are negative and decrease as steric hindrance increases because rotations in the R moiety that were free in the reactant system are hindered in the transitions states, the more so the larger the steric hindrance. What really distinguishes one transition state from the other is the vibrational contribution. Among the various frequencies involved, many are practically the same in the transition states, but a few of them are significantly different. For example, with MeCl + NO^-, each transition state has 15 normal vibration modes. One has a negative frequency, as expected for a transition state. Nine frequencies, corresponding to vibrations within the fragments, are the same in both cases. The difference in entropy comes from the five remaining frequencies, which feature the relative position of the fragments. These frequencies are smaller for the ET-TS than for the S_N2-TS. This greater looseness of the ET-TS as compared to the S_N2-TS thus makes the vibrational contribution to the activation entropy significantly larger in the first case than in the second (Table 2).

It is interesting to discuss in more detail the reaction pathways that connect each of the two transition states to products. For practical reasons, the determination of the steepest descent pathways according to the intrinsic reaction coordinate (IRC) method (see the Methodology section) and of the potential energy surface around points of interest can only be performed in the gas phase at the UHF level. We may thus disclose qualitative trends but not a quantitative description of the actual reaction pathways and of the competition between them. In the gas phase, the reactants and products form clusters that are more stable than the separated molecules. Their geometries are depicted in Scheme 3 (all structure details are given in the Supporting Information), and their energetics, at the UHF level, are summarized in Table 3, together with the values of the main geometrical parameters.

There are two reactant states. One, R, which correlates with the ET transition state, consists of separated molecules. The other, RC-S_N2, which has the same atom sequence as and correlates with the S_N2-TS, is significantly lower in energy than the separated molecule, reflecting the existence of a charge/dipole ($^{+\delta}$C- -Cl$^{-\delta}$) interaction.

In all cases, the IRC steepest descent pathway was found to connect the ET-TS to the separated reactants and the S_N2-TS to the S_N2 reactant cluster. The attack of NO^- is thus diametrically opposed in the ET and S_N2 reactions, respectively.

There is one S_N2 product cluster, S_N2-PC, but there are two ET product clusters that can both be obtained from the separated products. In one of the two, ET-PC (ET), the atom sequence is C Cl N. In the other, ET-PC (S_N2), the atom sequence is Cl C N. The latter system may be obtained by homolytic decomposition of the S_N2 product cluster or, as shown below, by a mechanism bifurcation following the S_N2-TS.

The ET-TS is connected in all cases with the ET-PC (ET) cluster. Once the separated ET products have been formed from this cluster, the radicals R$^\bullet$ and NO$^\bullet$ may easily combine to yield the substitution product, RNO. Note that in the case of a chiral reacting carbon, the racemic substitution product will be obtained along this reaction pathway, whereas inversion will take place along the direct S_N2 pathway.

It is not possible to represent both the S_N2 and ET pathways on a single potential energy surface as a function of the same two main coordinates. We may, however, follow the S_N2 pathway as a function of the C−Cl and C−N distances and see whether the reaction yields the S_N2 product or may, by means of a mechanism bifurcation, end up giving the ET-PC (S_N2) product cluster. We have carried out an IRC analysis of this question in all four cases (Figure 2).

Along the ET pathway, the N−O distance changes from 1.245 to 1.13 Å with a strong variation around the transition state, where it is equal to 1.20 Å. This behavior is pictured in Figure 2 for the Me and *t*-Bu cases, and the same has been found for the two other cases. At the transition state, the charge on NO is of the order of −0.65, and the R moiety possesses a strong radical character, as attested by a spin density on the carbon of the order of 0.75 (see table). The rapid variation of the N−O distance may thus be used as a signature of the occurrence of electron transfer.

In the Me case, the S_N2 IRC pathway connects the transition state to the S_N2 product cluster. The N−O distance passes from 1.245 to 1.21 Å with a smooth variation around the transition state, where it is equal to 1.225 Å. At the transition state, the charge on NO is large, −0.80, and the carbon has practically no radical character (spin density 0.07). This behavior strongly contrasts the ET behavior depicted earlier. Past the transition state, there is some tendency to electron transfer, as shown by the minimum in the d_{NO} curve (Figure 2). More charge has been transferred (the charge on NO is now −0.57), and the carbon exhibits some radical character (spin density 0.21). However, at this point the C−N bond is substantially formed (C−N distance 1.88 Å), and the complete formation of the bond proceeds smoothly from this point to the S_N2 product cluster. As found earlier in the reaction of formaldehyde anion radical with methyl chloride,[14b] electron transfer lies somewhat ahead of the formation of the bond, but these two steps overlap each other so much that they must be viewed as a single event.

Figure 3 shows the potential energy surface representing the S_N2 reaction as a function of the two coordinates, C−Cl and C−N. The surface was constructed from the optimization of ca. 200 structures. This was possible using a reasonable amount of computer time for the smallest system, MeCl + NO^-, but not for the three larger systems we have investigated. In Figure 3, the potential energy surface is represented as a function of the mass-weighted C−Cl and C−N coordinates (skew angle = 46.8°, $\gamma = 0.974$, see the Methodology section). The potential energy surface exhibits three valleys corresponding to the reactants, the S_N2 products, and the ET products, respectively. The reactant on one hand and the S_N2 and ET products valleys on the other hand are connected by a col (solid line in Figure 3). Its lowest point is a saddle point corresponding to the S_N2 transition state. The S_N2 products and the ET products valleys are connected by a col, the saddle point of which corresponds to the transition state of the homolytic dissociation RNO → R$^\bullet$ + NO$^\bullet$ and of the reverse coupling reaction. The IRC pathways going through these saddle points are also shown in Figure 3.

Scheme 3[a]

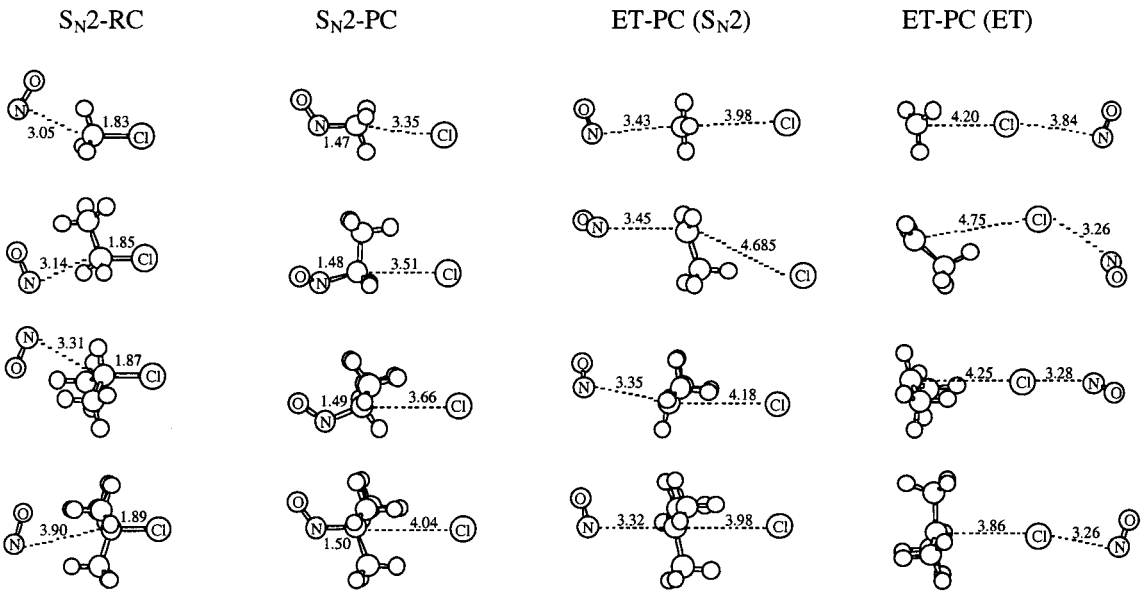

[a] RC, reactant cluster; PC, product cluster.

Table 3. Energetic and Geometric Characteristics of the Reactant and Product Clusters in the Gas Phase at the UHF Level[a]

	Me					Et				
	S_N2-RC	R	S_N2-PC	ET-PC (S_N2)	ET-PC (ET)	S_N2-RC	R	S_N2-PC	ET-PC (S_N2)	ET-PC (ET)
ΔE_{UHF}	−0.59	0.00	−1.675	−0.735	−0.73	−0.65	0.00	−1.70	−0.856	−0.81
d_{C-Cl}	1.826	1.77	3.35	3.98	4.20	1.85	1.78	3.51	4.685	4.75
d_{C-N} or d_{Cl-N}	3.04	∞	1.47	3.43	3.84	a∞	3.37	1.48	3.45	3.26
q_C	0.19	−0.01	0.34	0.00	0.00	0.14	−0.03	0.30	−0.055	−0.055
q_{Cl}	−0.245	−0.01	−0.98	−0.995	−0.995	−0.25	−0.01	−0.97	−0.975	−0.98
q_{N-O}	−0.945	−0.98	−0.36	0.00	0.00	−0.94	−0.98	−0.36	0.00	−0.01

	i-Pr					*t*-Bu				
	S_N2-RC	R	S_N2-PC	ET-PC (S_N2)	ET-PC (ET)	S_N2-RC	R	S_N2-PC	ET-PC (S_N2)	ET-PC (ET)
ΔE_{UHF}	−0.76	0.00	−1.74	−0.945	−1.03	−0.80	0.00	−1.78	−1.06	−0.93
d_{C-Cl}	1.865	1.79	3.66	4.18	4.25	1.89	1.80	4.04	3.98	3.86
d_{C-N} or d_{Cl-N}	3.305	∞	1.49	3.345	3.28	3.90	∞	1.50	3.315	3.255
q_C	0.07	−0.073	0.23	−0.015	−0.156	−0.06	−0.145	0.10	0.034	0.13
q_{Cl}	−0.253	−0.01	−0.96	−0.97	−0.96	−0.25	0.00	−0.95	−0.965	−0.98
q_{N-O}	−0.92	−0.98	−0.35	0.00	−0.013	−0.91	−0.98	−0.335	−0.01	−0.015

[a] The energies are in electronvolts and the distances in angstroms. ΔE_{UHF} was calculated taking as origin the separated reactants.

We may note incidentally that the approximations made for constructing the two-dimensional potential energy surface are correct since the two IRC pathways do follow the hollow of the corresponding valley. As shown in Figure 3 (dotted/dashed line), the ridge separating the S_N2 and the ET valleys starts from a point, B, located on the col connecting the reactant valley with the S_N2 and ET products valleys and goes through the transition state of the RNO homolytic dissociation, HD-TS. Out of the trajectories coming from the reactant state and passing through the col, some may pass over the ridge, reach the ET valley, and go down to the ET products. However, the ET side of the surface is high and rather flat, and the ridge separating this area from the S_N2 side is not very pronounced. As a consequence, the amount of ET products finally formed is predicted to be very small as compared to the S_N2 products.

In the Et and *i*-Pr cases, the IRC pathway also connects the S_N2 transition state to the S_N2 products. Along this S_N2 pathway, a minimum in the N−O distance is again observed which corresponds to an even smaller value of the N−O distance. Electron transfer thus lies ahead of bond formation in these two cases, too. However, bond formation shortly follows, thus preventing the IRC pathway from bifurcating toward the ET product. It is likely that a partition mechanism exists in these two cases, too, that allows some ET products to be formed after the passage of the S_N2 transition state. Actually, this mechanism is likely to be more efficient than in the Me case with Et and, even more, with *i*-Pr. In the case of a chiral reacting carbon, the partition mechanism will lead ultimately to partial racemization along the indirect ET pathway in addition to the inversion products formed along the S_N2 pathway. In the case of *i*-Pr, the direct ET pathway begins to compete efficiently with the S_N2 pathway (Figure 1). The indirect and the direct ET pathways may thus concur to the formation of racemic products. The latter situation is reminiscent of what was observed experimentally in the reaction of optically active 2-octyl halides with the anion radical of anthracene, in which the racemization yield was found to be ca. 90%,[2] although the reaction is faster than predicted for a direct outer-sphere dissociative electron transfer reaction.[7]

The *t*-BuCl reaction is remarkable in the sense that, unlike in the three other examples, the IRC pathway connects the S_N2 transition state to the ET products rather than to the S_N2 products (Figure 2). Past the S_N2 transition state, the N−O distance decreases rapidly to the value it has in $NO^{\bullet}$ in a way which is very similar to what happens with the same compound along

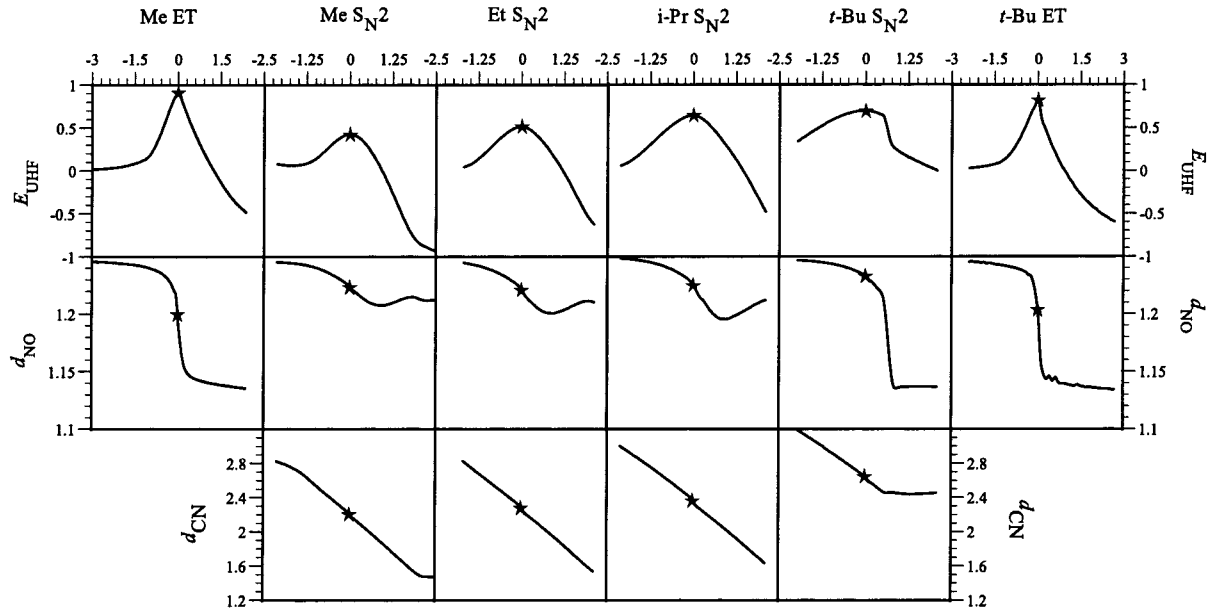

Figure 2. Variations of the energy and the N−O and C−N distances with the curvilinear coordinate along the S_N2 IRC pathway in all four cases and along the ET IRC pathway for Me (extreme left) and *t*-Bu (extreme right). Energies in electronvolts, distances in angstroms. The star on each curve indicates the transition state.

the direct ET pathway. Figure 4b gives a more detailed view of this bifurcation in a two-dimensional representation (vs the mass-weighted C−Cl and C−N coordinates), while the pathways for MeCl are recalled in Figure 4a for comparison. In Figure 4b, past the S_N2 transition state, the surface does not divide into an S_N2 valley and an ET valley until point B is reached. The ridge separating the two valleys (dashed line) starts from this point and ends at the transition state of the homolytic dissociation reaction (HD-TS). As expected, the IRC pathway stays on the ridge for a short while[15g] and then bifurcates toward the ET valley. Although the S_N2 product cluster is lower in energy than the ET product cluster, the descent is steeper in the second case than in the first.

Electron transfer products are thus formed both by an indirect pathway after passing through the S_N2 transition state and by the direct ET pathway passing through the ET transition state, which now tends to be lower in energy than the S_N2 transition state. The electron transfer reaction thus takes place from the rear side, from the front side, and also from other sides since the *t*-Bu case is characterized by large vibrational entropies for both the ET and the S_N2 transition states (Table 2). Thus, because of steric hindrance, all directions of attack lead to single electron transfer with similar activation energies and with similar reacting distances. We may thus average all the transition states corresponding to the various directions to form an overall transition state with no privileged direction of attack and in which the bonded interaction between the reacting carbon and the nucleophile is negligible.[20] This picture corresponds precisely to the concept of outer-sphere electron transfer, for which the Marcus−Hush model[21] has been conceived when no bond is broken and for which the Morse curve dissociative electron transfer model[4b] has been proposed when a bond is broken in concert with electron transfer, as is the case here.

Methodology

All calculations were carried out with the Gaussian 94 and 98 programs.[22] The 6-31G* basis set was used. All geometries were fully optimized without symmetry restriction at the UHF level. Convergence on the lowest electronic structure was tested with the option STABLE. Frequency calculations were made at the optimized geometries to verify that the structures were minima (no imaginary frequencies) or saddle points (one imaginary frequency). Single-point energy calculations at the MP2/6-31G* level of theory were performed at these geometries in order to introduced correlation energy. Inner shells were excluded from the correlation energy calculations (frozen-core approximation). Geometries of the stationary points of the MeCl + NO^- system were also fully optimized at the MP2 level, and frequency calculations were made on these structures at this level.

The UHF/6-31G* geometries and vibrational frequencies were used to evaluate the various thermodynamic parameters for the stationary points, including the zero-point energy (ZPE), the vibrational correction to the ZPE at 298 K, the rotational and translational energies, the *PV* terms (determined as *nRT*), and the entropy from the usual relationship

(20) For the following reasons: The C- -Nu bonded interaction varies from weak for the rear-side attack to nil from the front-side attack. Because of their respective energies, the weight in the average varies from maximal to minimal from the latter to the former. Combination of the two factors leads to the conclusion that the overall C- -Nu bonded interaction may be neglected.

(21) (a) Marcus, R. A. *J. Chem. Phys.* **1956**, *24*, 4966. (b) Hush, N. S. *J. Chem. Phys.* **1958**, *28*, 962.

(22) (a) Frisch, M. J.; Trucks, G. W.; Schlegel, H. B.; Gill, P. M. W.; Johnson, B. G.; Robb, M. A.; Cheeseman, J. R.; Keith, T.; Petersson, G. A.; Montgomery, J. A.; Raghavachari, K.; Al-Laham, M. A.; Zakrzewski, V. G.; Ortiz, J. V.; Foresman, J. B.; Cioslowski, J.; Stefanov, B. B.; Nanayakkara, A.; Challacombe, M.; Peng, C. Y.; Ayala, P. Y.; Chen, W.; Wong, M. W.; Andres, J. L.; Replogle, A. S.; Gomperts, R.; Martin, R. L.; Fox, D. J.; Binkley, J. S.; Defrees, D. J.; Baker, J.; Stewart, J. P.; Head-Gordon, M.; Gonzalez, C.; Pople, J. A. *Gaussian 94*, Revision E.1; Gaussian, Inc.: Pittsburgh, PA, 1995. (b) Frisch, M. J.; Trucks, G. W.; Schlegel, H. B.; Scuseria, M. A.; Gill, P. M. W.; Johnson, B. G.; Robb, M. A.; Cheeseman, J. R.; Keith, T.; Petersson, G. A.; Montgomery, Stratmann, R. E.; Burant, J. C.; Dapprich, S.; Millam, J. M.; Daniels, A. D.; Kudin, K. N.; Strain, M. C.; Farkas, O.; Tomasi, J.; Barone, V.; Cossi, M.; Cammi, R.; Mennuci, B.; Pomelli, C.; Adamo, C.; Clifford, S.; Ochterski, G.; Cui, Q.; Morokuma, K.; Malick, D. K.; Rabuck, A. D.; J. A.; Raghavachari, K.; Al-Laham, M. A.; Zakrzewski, V. G.; Ortiz, J. V.; Foresman, J. B.; Cioslowski, J.; Stefanov, B. B.; Liu, G.; Liashenko, A.; Piskorz, P.; Komaromi, I.; Nanayakkara, A.; Challacombe, M.; Peng, C. Y.; Ayala, P. Y.; Chen, W.; Wong, M. W.; Andres, J. L.; Replogle, A. S.; Gomperts, R.; Martin, R. L.; Fox, D. J.; Binkley, J. S.; Defrees, D. J.; Baker, J.; Stewart, J. P.; Head-Gordon, M.; Gonzalez, C.; Pople, J. A. *Gaussian 98*, Revision A.1; Gaussian, Inc.: Pittsburgh, PA, 1998.

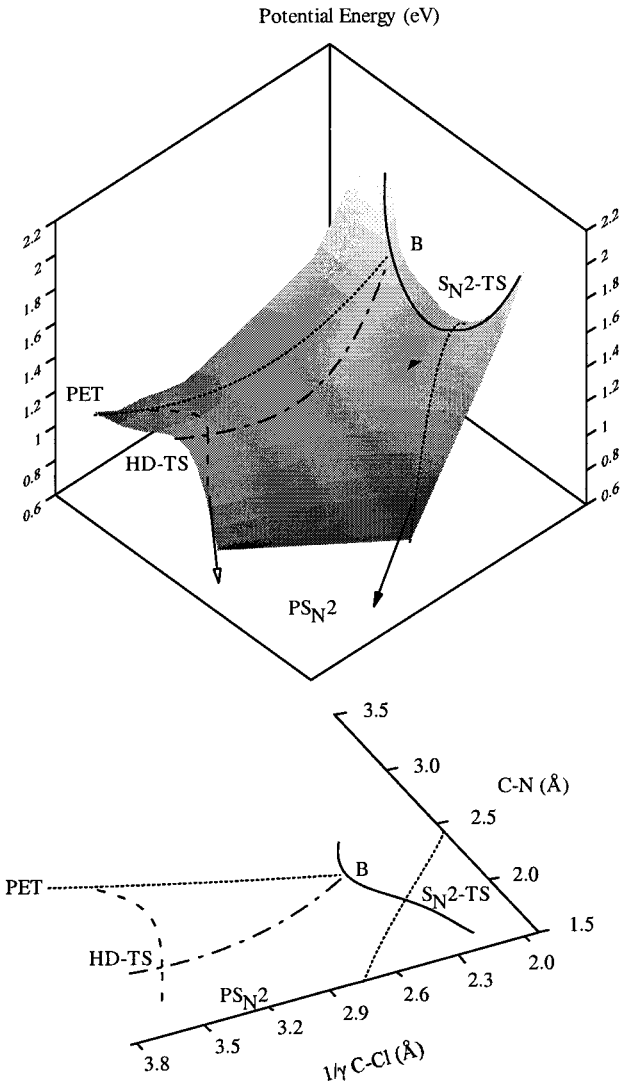

Figure 3. MeCl + NO^-. Top: Potential energy surface representing product valleys of the S_N2 reaction as a function of the two coordinates, $1/\gamma$ C−Cl and C−N (skew angle 46.8°, $\gamma = 0.974$), the reactant system being located behind the surface shown. Full line: Col separating the reactant and product valleys. Dotted lines: IRC S_N2 pathway and steepest descent pathway from point B to the ET products. Dashed line: Ridge separating the S_N2 and ET products valleys. Dashed/ dotted line: Ridge separating the S_N2 and ET valleys. Bottom: Projection of the reaction pathways, ridge, and col on the $1/\gamma$ C−Cl/C−N plane with the same skew angle and γ value as above. S_N2-TS, S_N2 transition state; HD-TS, homolytic transition state; PS_N2, S_N2 products; PET, electron transfer products; B, starting point of ridge separating the S_N2 and ET products valleys.

within ideal gas, rigid rotor, and harmonic oscillator models.[23] The same calculations were also made at the MP2 level for the MeCl + NO^- system.

The charges and spin densities on the main atoms were obtained by a Mulliken population analysis.

Reaction Paths. The nature of the reactants and products linked to the transitions states was assigned by the intrinsic reaction coordinate (IRC) method[24] at the HF level. The IRC has been determined in mass-weighted internal coordinates (which is equivalent to mass-weighted Cartesian coordinates) with a step size of 0.20 or 0.10 in atomic units. The IRC is then the path of steepest descent and can be defined as the path followed by a classical particle sliding with infinitesimal velocity from a saddle point down to each of the minima.[25]

(23) McQuarrie, D. A. *Statistical Mechanics*; Harper and Row: New York, 1976.

(24) Gonzalez, C.; Schlegel, H. B. *J. Phys. Chem.* **1990**, *94*, 5523.

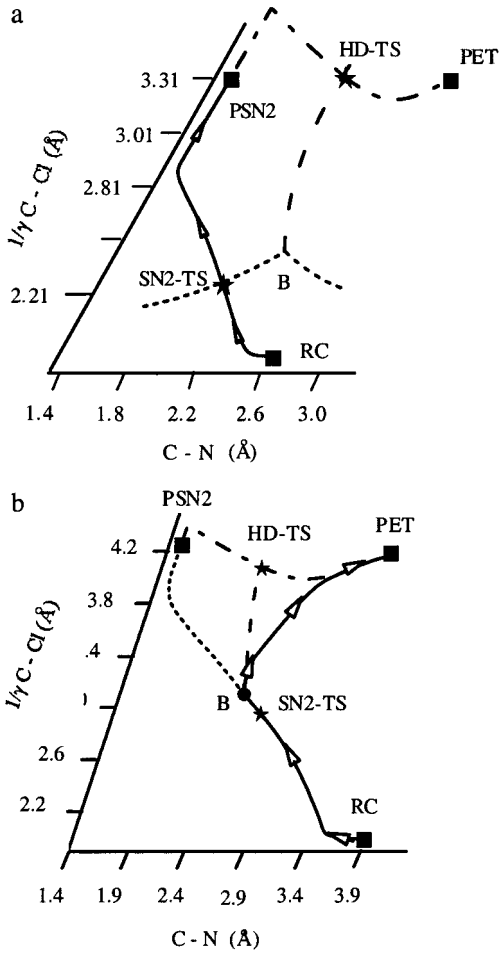

Figure 4. Reaction pathways in the reactions of methyl chloride (a) and *tert*-butyl chloride (b) with NO^-. ■, reactant and products; ★, transition states. In a and b, the full line is the mass-weighted IRC path from the reactant to the product states, the dashed line is a ridge separating the S_N2 and ET valleys, and the dotted-dashed line is the mass-weighted IRC path from the S_N2 product state to the ET product state (homolytic dissociation). The dotted line in a represents the col separating the reactant and the S_N2 product valleys. The dotted line in b represents the steepest descent path from the bifurcation point, B, to the S_N2 product. In a, B is the point of the col separating the reactant and the S_N2 product valleys where the ridge separating the S_N2 and ET valleys starts. Skew angle, 46.8° (a), 68.7° (b); $\gamma = 0.974$ (a), 0.948 (b).

To examine the potential energy surface relevant to the S_N2 pathway for the MeCl + NO^- system, we have constructed a two-dimensional subspace. Two distances were fixed (C−Cl and C−N) while the other geometrical parameters were optimized but with a symmetry restriction: in MeCl, the three angles formed with chlorine, carbon, and hydrogen atoms remained equal. The energies of approximately 200 points were calculated. The depiction of the region where electron transfer occurs necessitated a finer mesh than in the other regions. A surface in skewed axes (mass-weighted and scaled) was then plotted. This coordinate system has special significance for the reaction dynamics. Indeed, the dynamics of the reaction is represented by means of a point mass moving over the potential energy surface.[26a] For the MeCl + NO^- system, a good approximation to the mass weighting can be obtained by considering the reaction as a collinear triatomic reaction with NO, Me, and Cl as the three fragments. The scale factor γ and the skew angle β between the axes are thus obtained using the masses of these fragments.[26]

(25) Fukui, K. *Acc. Chem. Res.* **1981**, *14*, 363.

(26) (a) Glasstone, S.; Laidler, K.; Eyring, H. *The Theory of Rate Processes*; McGraw-Hill: New York, 1941. (b) $\gamma = [m_{NO}(m_R + m_{Cl})/m_{Cl}(m_{NO} + m_R)]^{1/2}$ and $\cos\beta = [m_{NO}m_{Cl}/(m_R + m_{NO})(m_R + m_{Cl})]^{1/2}$ (β is the skew angle between the axes).

Table 4. $MeCl + NO^-$: UHF and MP2 Geometries, Energies, and Free Energies[a]

	E		G^{gp}		G^{solv}		G^{s}		d_{C-Cl}		d_{C-N} or d_{Cl-N}		d_{N-O}		q_{N-O}		s_C	
	UHF	MP2	eq 1	MP2	UHF	MP2	eq 3	MP2	UHF	MP2	UHF	MP2	UHF	MP2	UHF	MP2	UHF	MP2
R	0.00	0.00	0.00	0.00	−3.37	−3.36	0.00	0.00	1.785	1.780	∞	∞	1.248	1.281	−1	−1	0.00	0.00
$^3PS_N2$	−1.22	−1.05	−1.09	−0.86	−3.33	−3.30	−0.80	−0.79	∞	∞	1.457	1.459	1.220	1.218	−0.27	−0.29	0.00	0.00
$^1PS_N2$	−1.32	−2.10	−1.12	−1.95	−3.27	−3.26	−1.69	−1.85	∞	∞	1.464	1.481	1.177	1.236	−0.22	−0.25	0.00	0.00
PET	−0.70	−0.20	−1.18	−0.53	−3.18	−3.18	−0.43	−0.29	∞	∞	∞	∞	1.127	1.143	0.00	0.00	1.00	1.00
$^3S_N2$-TS	−0.16	−0.34	0.20	0.035	−2.41	−2.46	0.94	0.88	2.231	2.139	2.208	2.174	1.224	1.258	−0.80	−0.83	0.07	0.02
$^1S_N2$-TS (sp)[b]	2.37	0.135	–	–	–	–	–	–	–	–	–	–	–	–	–	–	–	–
$^1S_N2$-TS	1.40	–	1.85	–	−2.42	–	1.80	–	2.010	–	2.477	–	1.219	–	−0.83	–	0.00	–
ET-TS	1.101	0.58	1.20	0.80	−2.70	−2.76	1.32	1.35	2.148	2.117	2.472	2.363	1.200	1.212	−0.63	−0.72	0.77	0.675

[a] Energies are in electronvolts and distances in angstroms. [b] Single-point calculation of the energy of the singlet in the geometry of the triplet.

Solvation. Solvation free energies were calculated on the gas-phase conformations optimized at the UHF level according to the SCRF (self-consistent reaction field) method using the COSMO[27a] and IPCM models[27b,c] at the MP2 level. In these methods, the solvent is treated as a continuum of uniform dielectric constant ϵ_r (here, $\epsilon_r = 36$), in which the solute is placed into a cavity of molecular shape, and the reaction field is described in terms of apparent polarization charges or reaction field factors included in the solute Hamiltonian. In the IPCM model, the definition of the cavity is based on an isosurface of the total electron density calculated at the level of theory being applied (here MP2). In the COSMO approach, the solute molecules are embedded in cavities formed by interlocking spheres centered on the solute atoms. The surface is smoothed by adding some other spheres to simulate the solvent-excluding surface.

Conclusions

The following features of the S_N2/ ET dichotomy and connections emerge from our ab initio quantum mechanical investigation of the $RCl + NO^-$ model reaction varying R from methyl to ethyl, isopropyl, and *tert*-butyl.

Distinct S_N2 and ET transition states are identified on the potential energy hypersurface in all cases. In the methyl case, the latter is higher in free energy than the former, thus disfavoring the ET pathway. As steric hindrance increases, the S_N2 activation free energy increases while the ET activation free energy does not vary much. The result is that the balance is increasingly in favor of the ET reaction, which becomes predominant in the *tert*-butyl case. The geometries of the two transition states are drastically different, being characterized by an N C Cl atom sequence in the S_N2 transition state and a C Cl N sequence in the ET transition state. In the first case, the main directionality factor is the interaction between the negatively charged electron donor and the partial positive charge borne by the reacting carbon. In the second, the predominating factor is the overlap between the σ^* orbital of the C−Cl bond, which is mostly located on Cl, and the electrons on the NO^- nitrogen which fights successfully electrostatic repulsion.

One factor which favors the ET reaction in all cases is the looseness of its transition state and the lesser directionality of attack as compared to the S_N2 case. These factors translate into a larger vibrational entropy of activation in the ET reaction as compared to the S_N2 reaction.

While the ET transition state connects with the ET products, this is not always the case with the S_N2 reaction. In the methyl case, the steepest descent pathway connects the S_N2-TS to the S_N2 products. The possibility of a partitioning between this pathway and an indirect ET pathway leading to an N C Cl cluster (instead of the C Cl N cluster obtained from the direct electron transfer reaction) exists at the level of the col connecting the reactant valley to the S_N2 and ET product valley. However, the ratio of ET products formed in this way appears negligible. Upon increasing steric hindrance, the steepest descent pathway still connects the S_N2-TS to the S_N2 products in the ethyl and isopropyl cases, but the formation of ET products along the indirect ET pathway is expected to increase. The *tert*-butyl case represents an extreme situation where the S_N2 transition state is connected with the ET products rather than with the S_N2 products, while the direct ET pathway becomes more facile than the S_N2 pathway. All directions of attack lead to single electron transfer with similar activation energies, with similar reacting distances and negligible carbon−nucleophile bonded interactions in the transition state. This reaction thus offers a good illustration of an outer-sphere process as conceived in previous models of dissociative electron transfer.

Acknowledgment. One of us, C.C., is grateful to the Centre de Supercomputacio de Catalunya for the attribution of a fellowship (Training and Mobility of Researchers Program) that allowed him to start its training in quantum chemistry under the expert guidance of Prof. Juan Bertran and Dr. Miquel Moreno (Universitat Autonoma de Barcelona) in September 1997.

Appendix

As shown in Table 4, the characteristic free enthalpies obtained at the MP2/6-31G*//UHF/6-31G* level are close to the more accurate values obtained at the MP2/6-31G* level.

We also see from Table 4 that the triplet state is more stable than the singlet state for all points or portions of interest of the potential energy hypersurface.

Supporting Information Available: UHF/6-31G* and MP2/6-31G* structure details in Gaussian archive format (PDF). This material is available free of charge via the Internet at http://pubs.acs.org.

JA993467M

(27) (a) Barone, V.; Cossi, M. *J. Phys. Chem. A* **1998**, *102*, 1995. (b) Foresman, J. B.; Frisch, A. *Exploring Chemistry with Electronic Structure Methods*; Gaussian Inc.: Pittsburgh, PA, 1996. (c) Foresman, J. B.; Keith, T. A.; Wiberg, K. B.; Frisch, M. J. *J. Phys. Chem.* **1996**, *100*, 16098.